Truncated Ditetragonal Gold Prisms as Nanofacet Activators of Catalytic Platinum

8 **AUTHORS**, INCLUDING:

Yugang Zhang
Brookhaven National Laboratory
24 PUBLICATIONS **574** CITATIONS

Jia Wang
Brookhaven National Laboratory
106 PUBLICATIONS **4,703** CITATIONS

Eric Andrew Stach
Brookhaven National Laboratory
392 PUBLICATIONS **15,152** CITATIONS

Oleg Gang
Brookhaven National Laboratory
123 PUBLICATIONS **2,782** CITATIONS

Truncated Ditetragonal Gold Prisms as Nanofacet Activators of Catalytic Platinum

Fang Lu,*,[†] Yu Zhang,[‡] Lihua Zhang,[†] Yugang Zhang,[†] Jia X. Wang,[‡] Radoslav R. Adzic,[‡] Eric A. Stach,[†] and Oleg Gang*,[†]

[†]Center for Functional Nanomaterials and [‡]Chemistry Department, Brookhaven National Laboratory, Upton, New York 11973, United States

S *Supporting Information*

ABSTRACT: We report a facile, seed-mediated method to synthesize nanoscale gold truncated ditetragonal nanoprisms (TDPs) enclosed by 12 high-index {310} facets. The method leads to the formation of nanoparticles with high size and shape monodispersity and allows for easy surfactant removal. The dependence of particle shape on the synergetic contribution of metallic ions, halide ions, and surfactant adsorbates during synthesis is described. The resulting high-index nanoparticle facets were demonstrated as efficient activators of a supported catalytic material (platinum). A Pt monolayer deposited onto the Au TDP nanofacets with sharp electrochemical signatures exhibits an enhanced catalytic activity.

Surfaces and surface structure determine many of the physical and chemical properties of crystalline matter.[1,2] Substantial recent research regarding nanoparticle (NP) synthesis has been devoted to controlling the shape of nanoscale objects. Such particles possess well-defined crystallographic facets, which allows for tuning of their surface-dependent properties.[1,2] In particular, high-index-faceted metal NPs are of great interest due to their potential use in plasmonic and catalytic applications.[3–8]

The synthesis of metallic NPs through control of the growth of low-index facets such as {111} and {100} results in NPs with well-defined shapes, such as cubes, octahedra, and rods.[2] In contrast, expression of high-index facets on metallic NPs can permit formation of more complex shapes with higher surface reaction activity. Indeed, a large density of atomic steps and terraces on high-index facets is greatly desirable for breaking and forming chemical bonds during catalytic reactions.[1d] However, the low stability of these surfaces leads to their easy disappearance during crystal growth.[1d,3] In the case of gold NPs in particular, only limited systems with high-index facets—such as trisoctahedra (TOH),[4] tetrahexahedra (THH),[5] and concave cubes[6a]—have been prepared. To shape and stabilize nanofacets, the organic molecules or polymers are used as surface capping agents and inevitably accompany the growth of high-index-faceted NPs.[4–8] These surfactants usually possess a strong affinity to the confined NPs surfaces and unavoidably passivate the desired surface activity from high-index nanofacets in the form of residue.[7,9] The electrochemical activity of high-index-faceted NPs is highly sensitive to the purity of the nanofacets, as evidenced in previous studies.[4–6]

We explore here how the facets of shaped NPs can be used as an atomically structured support for a monolayer (ML) of catalytically active materials. Such a material design strategy allows for modulation of both the structure and properties of the deposited ML. This approach is distinct from existing, state-of-the-art core/shell synthesis methods where surface features are typically not replicated during the shell formation[10,11] Herein, we report a facile seed-mediated route, selecting cetylpyridinium chloride (CPC) as a surfactant, to synthesize well-shaped Au truncated ditetragonal nanoprisms (TDPs) in high purity. The method provides a high-yield (>95%) synthesis of uniform ∼45 nm Au TDP NPs, which are bounded by 12 high-index {310} facets. We demonstrated a distinct electrochemical feature from Au nanofacets, suggesting the effective removal of surface capping agents. Furthermore, the Au TDP NPs were successfully used as stable facet-specific supports for platinum ML deposited onto the underlying Au nanofacets. Pt exhibited a high electrochemical catalysis activity, which was activated by high-index-facet features.

In a typical synthesis, Au seeds were injected into a growth solution containing $HAuCl_4$, $AgNO_3$, HCl, ascorbic acid (AA), and CPC under magnetic stirring. The mixed solution was left undisturbed overnight (Supporting Information). Figure 1 shows scanning electron microscopy (SEM) images of the NPs obtained from a reaction wherein 50 μL of the diluted seeds was added, equivalent to 1 μL of the original seed solution. The X-ray powder diffraction (XRD) pattern of the as-prepared NPs (Figure S1a) matches the FCC gold structure (JCPDS 4-0784). Due to their high monodispersity, the uniform particles can self-assemble into ordered and well-packed structures, as evident from the low-magnification SEM image (Figure 1a). Our high-magnification observations (Figure 1b,c) reveal well-defined facets with an average long edge length of ∼45 nm. These NPs exhibit a ditetragonal prism shape with truncated ends, smaller than the ones reported recently.[7] They are enclosed by 12 facets, including eight side facets parallel to the principal axis and two terminating facets located at each of the two ends (Figure 1c). The schematic drawing of TDP indicates the projections along three orthogonal viewing directions (Figure 1d), which is in agreement with the observed particle profiles (Figure 1e$_1$–e$_3$). SEM images of the particles when surrounded by neighboring NPs show that the particles have a ditetragonal cross-section (Figure 1e$_1$). The measured inner angles match closely those calculated from an
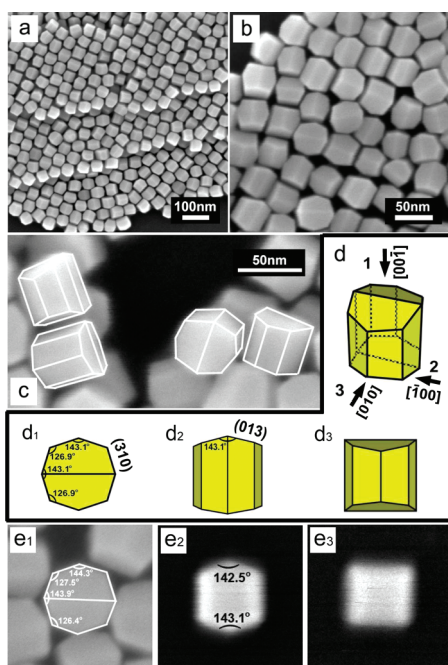
Figure 1. (a) Typical large-area and (b) locally magnified SEM images of the as-prepared Au TDP NPs, with an edge length of 45 ± 4 nm. (c) High-magnification SEM image stressing typical TDP profiles in random orientations. (d) Model of an ideal TDP bound by {310} facets and projections along three viewing directions indicated with arrows, as shown in d_1-d_3. (e) High-magnification SEM images of single NP in different orientations, corresponding to the TDP models in d_1-d_3. The frame scale in e_1-e_3 is 80 nm.

Figure 2. TEM images, schematic models, and electron diffraction patterns of single TDP Au NP orientated along the (a_1-a_3) [001], (b_1-b_3) [013], (c_1-c_3) [010], and (d_1-d_3) [03$\bar{1}$] axes. Scale bar, 20 nm.

ideal TDP with high-index {310} side facets (Figure 1d_1); similarly, a side-view projection (Figure 1e_2) exhibits measured angles between edge-on facets at the two ends of the prism which also agree with expected values for {310} facets (Figure 1d_2).[7] These measurements indicate that the synthesized Au NPs have a TDP shape bound by {310} facets. By varying the volume of seed particles added to the growth solution, the size of the Au TDP NPs—namely the length of the longest edge—can be adjusted. For example, Au TDP NPs with the edge length of ~72 nm were synthesized by adding an equivalent of 0.25 μL of the non-diluted seed solution, all while maintaining the TDP shape and high yield (>95%) (Figure S1b).

We have further investigated the shape and internal structure of Au TDP NPs using transmission electron microscopy (TEM). Figure 2 presents four representative TEM images of the NPs (Figure 2a_1, b_1, c_1, and d_1) together with the corresponding selected area electron diffraction (SAED) patterns (Figure 2a_3, b_3, c_3, and d_3) which demonstrate the NP orientation. The measured projected contours of NPs match the profiles of the ideal TDP in different orientations (Figure 2a_2, b_2, c_2, and d_2). When viewed along the [001] direction, the angle between the two end faces of the TDP is visible and can be used to determined the plane indices of the end faces as {310} (Figure 2a_1-a_3). The SAED patterns and high-resolution TEM (HRTEM) analysis (Figures 2c and S2) confirm that the principal axis parallel to the eight side faces is [100]. All the side-views can be obtained by rotating a TDP with the eight {310} side faces around the [100] principal axis. Combined with the SEM analysis, these structural characterizations confirm that the Au NPs are defect-free single-crystalline TDPs enclosed by 12 high-index {310}
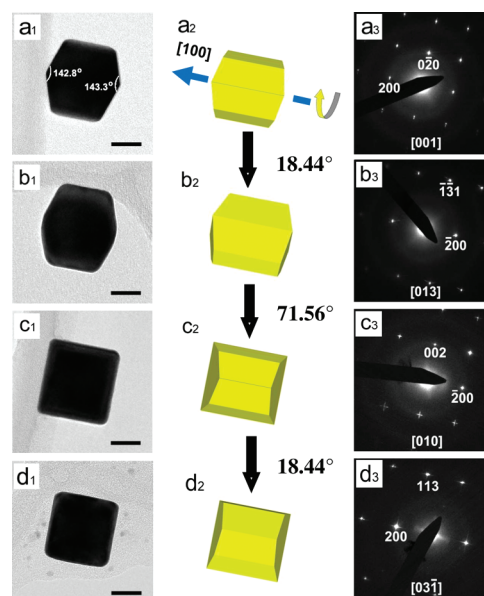
facets. The majority of the Au NPs exhibited this standard TDP shape (as illustrated in Figure 1d). A minority of NPs showed slight shape differences, but they were still bounded by 12 {310} facets (Figure S3).[7a] In the UV–vis absorption spectrum, the as-prepared Au TDP NPs exhibit only one strong surface resonance (SPR) peak at 545 nm (Figure S4). The spectrum feature differs from that of the TDP NPs reported previously, which shows two broad peaks corresponding to the transverse and longitudinal SPR modes.[7a] The difference would arise from the more symmetric aspect ratio and narrow size distribution of the Au TDP NPs presented here.

Several control experiments were carried out to probe the mechanism of Au TDP NPs formation. Under the present condition, which yields a low generation rate of Au atoms, the selective face-blocking effect from adsorbates is found to dominate the growth kinetics.[2b] Without adding both Ag$^+$ and HCl, but keeping all other experimental conditions unchanged, octahedral Au NPs bound by {111} facets were produced (Figure 3a), suggesting that the low-energy {111} facets are retained by CPC capping in the thermodynamically controlled reaction.[2b] Even when only HCl was added, octahedral Au NPs were still formed relatively slowly due to the decreased reducing power of AA after adding HCl (Figure 3b).[5] However, when only Ag$^+$ was added, rhombic dodecahedra NPs bound by {110} facets were obtained (Figure 3c). This indicates that the effect of Ag underpotential deposition (UPD) becomes dominant over the surfactant effect from CPC after introducing Ag$^+$, due to a relatively low binding affinity of CPC for Au surfaces.[2c,d] Ag$^+$ can be considered as a selective face-blocking adsorbate through the UPD mechanism, and it has been used in other solution-based syntheses to stabilize high-index facets.[12] The difference in the onset of Ag$^+$ UPD for various crystalline facets of Au leads to the preferable deposition of Ag on a Au surface in the order {110} > {100} > {111}. Therefore, a Ag ML can be formed more favorably on the Au {110} facets. The repeated galvanic reaction of a Ag ML by Au ions would significantly retard the total growth of the Au {110} facets.[12] A Ag
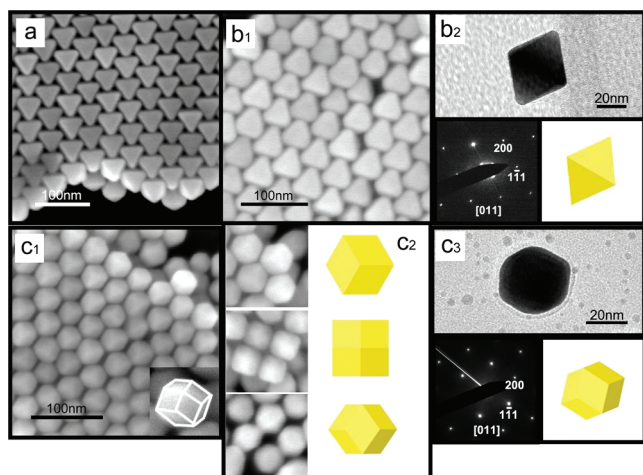
Figure 3. SEM images showing typically ordered assemblies of Au NPs prepared (a) without adding both HCl and AgNO$_3$ ({111}-facet-bounded octahedral NPs, OC) and (b$_1$) with adding HCl but no AgNO$_3$ (OC). (b$_2$) TEM image, diffraction pattern, and model of an octahedron in sample (b$_1$). (c$_1$) SEM images of Au NPs prepared with adding AgNO$_3$ but no HCl ({110}-facet-bounded rhombic dodecahedral NPs, RD). The inset shows an overview of a single NP. The frame scale of the inset is 50 nm. (c$_2$) Local SEM images and models of the RD NPs in various orientations. The frame scale of the inset is 100 nm. (c$_3$) TEM image, diffraction pattern, and model of a RD NP in sample (c$_1$).
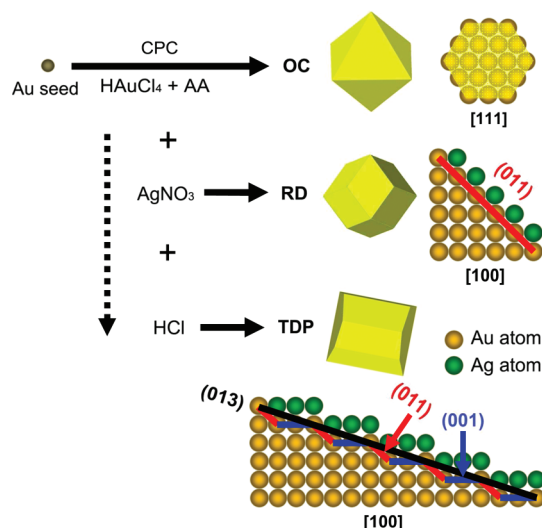

Figure 4. (Top) Schematic illustration of the formation mechanism of Au NPs (OC, RD, and TDP) bound by different index facets ({111}, {110}, and {310}, respectively), and the corresponding atomic models of these facets viewed along some given zone axis. The role of Ag monolayer UPD in the formation of Au {110} and {310} facets was also illustrated. (Bottom) Atomic model of the (013) facet of a TDP NP, projected from the [100] direction, showing that the (013) facet can be thought of as a combination of (001) terraces and (011) steps.

ML or sub-ML on the Au {110} facets acts as a strongly binding surfactant that results in a slower growth of Au {110} facets. This becomes dominant in determining the final NP structure.

By adding both Ag$^+$ and HCl, TDP NPs bounded by 12 {310} facets were obtained. The {310} facets are multiply stepped and can be considered as the vector sum of one {110} facet and two {100} facets.[7] It is believed that the cooperative action of Ag$^+$ and HCl would promote the Ag$^+$ UPD on the Au {100} facets and increase the proportion of Au {100} facets in the final structure. Meanwhile, the steps formed by sub-facets provide open sites with a larger UPD shift for Ag deposition and can be stabilized by Ag,[8,12] resulting in the unique TDP shape. Such a synergetic role of Ag$^+$ and HCl was also indicated in the seed-mediated syntheses reported recently.[2c,d,5,6a,7b,8] In these prior studies, combining Ag$^+$ and HCl led to the formation of Au THH NPs bound by 24 {730} facets (the vector sum of three {110} facets and four {100} facets)[5] and concave cubic NPs bound by 24 {720} facets (the vector sum of two {110} facets and five {100} facets).[6a] Note that different surfactants, either cetyltrimethylammonium bromide (CTAB), cetyltrimethylammonium chloride (CTAC), or CPC, were used in the synthesis of Au nanostructures bounded by different high-index facets. These results indicate that the type of surfactant is also crucial to determining the proportion of {110} and {100} sub-facets present in the high-index facets. Thus, the formation of the Au TDP NPs can be attributed to the synergistic function of Ag$^+$, halide ions, and the surfactant CPC (Figure 4). Efforts aimed at understanding synergistic roles of all compounds are ongoing.

The surface structure of the Au TDP NPs was also confirmed by electrochemical measurements. Au surface oxidation at potentials above 1.2 V is facet-sensitive. While a single large current peak occurs during cyclic voltammetry (CV) on close-packed Au {111} facets, multiple small peaks (not separated) characterize more open structures, such as {100}, {110}, and higher indexed facets.[13] The CV curve for the Au TDP NPs (blue) in Figure 5a exhibits three clear and small peaks (marked with a blue dashed frame), consistent with its well-defined high-index facets. Such distinct electrochemical surface features from Au TDP nano-facets confirm their high surface purity. This result also verifies that the surfactants (CPC) have been removed from the NPs surfaces by ethanol-washing and that the high-index facets remain intact. Otherwise, CV curves were found featureless.

The clean and stable crystalline profile of the Au TDP NPs was further examined as a facet-specific support for catalytically active metals, specifically Pt. A Pt ML was placed on the surface via galvanic replacement of an underpotentially deposited Cu ML.[14] We have previously demonstrated the formation of complete Pt ML, bilayer, and multilayer shells on <10-nm Pd NPs using Z-contrast STEM and element-sensitive EELS.[15] In this case, however, because Pt and Au are only different by one atomic number, and because the core particles are significantly thicker, we are not able to use Z-contrast to directly probe the structure of the Pt layer and its coverage. Nevertheless, electrochemical behaviors described below suggest that the deposited Pt is of ML thickness, with facets matching to the underlying Au. Indeed, the smaller Au reduction peak at 1.15 V and an additional reduction peak at 0.7 V in the voltammetry curve for the Au(TDP)-Pt(ML) sample (red curve in Figure 5a) are consistent with the presence of a Pt ML that partly shifts the reduction of surface oxide below 0.9 V, as commonly seen on Pt surfaces. For the Au(TDP)-Pt(ML) sample, the hydrogen desorption peak at 0.3 V is higher than that at 0.15 V (marked with a red dashed frame in Figure 5b), distinctly differing from the ratio of the two peaks in the CV curve for sphere-like Pt NPs (45% Pt/C were purchased from E-TEK), as shown in Figure 5b. This feature suggests that Pt ML lattice is not a hexagonal close-packed surface ({111}), but mimics the underlying Au NPs containing rich {100} sub-facets.[9] From the integrated hydrogen desorption

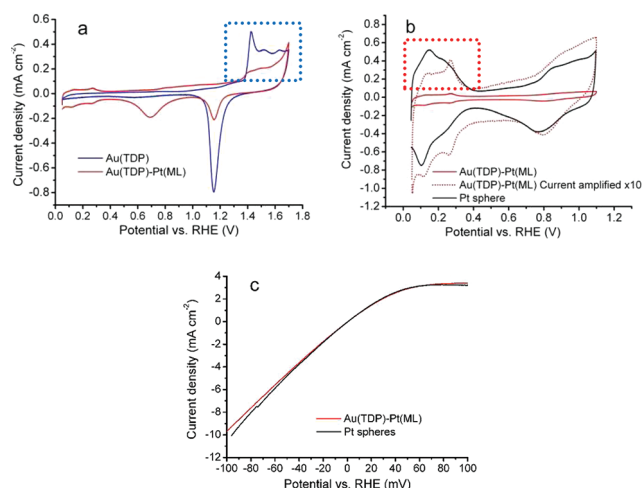**Figure 5.** (a,b) CV curves in deaerated 0.1 M H_2SO_4 solutions, 50 mV s^{-1}. (c) Polarization curve in hydrogen-saturated 0.1 M H_2SO_4 solutions, 5 mV s^{-1}, and 2500 rpm rotation rate. The current densities were normalized by the geometry area of the 0.5-cm-diameter electrode surface.

charges, the ratio between electrochemical surface areas of the Au(TDP)-Pt(ML) and the Pt NPs samples is estimated to be 1:20. This is largely because the Pt NPs are much smaller (average diameter about 2.5 nm) and, thus, have much higher Pt surface area. Yet, the polarization curves for hydrogen evolution and oxidation reactions are similar (Figure 5c), which indicates that the Pt ML on the high-index facets is much more active per Pt surface area than the close-packed surface of spherical Pt NPs. In other words, Au TDPs serve as nanofacet-activating substrates by translating their high-index-facet features to the supported materials; that results in a high electrochemical catalysis activity of the added Pt ML. The results illustrate a feasible way to study facet-dependent catalytic behavior of reactive metals using well-shaped Au NPs as facet-specific supports, as well as creating new opportunities for an enhancement of catalytic properties.

In summary, we developed a facile yet effective seed-mediated method which produces a high yield of Au NPs with a well-defined truncated ditetragonal prism shape at room temperature. The monodisperse Au TDP NPs are single crystals enclosed by 12 high-index {310} facets. High-indexed surfaces of the Au TDP NPs leave a distinct electrochemical feature when surfactants are removed from the NP surface. Furthermore, Au TDP NPs can be successfully used as stable, facet-specific supports, with high-index-facet features that readily allow for placement of a Pt monolayer and promote its catalytic performance. This work demonstrates that high-index-faceted Au NPs can be obtained by appropriately combining metallic ions, halide ions, and surfactant adsorbates in the seed-mediated synthesis. These NPs can replicate their specific surface features to the supported layer and function as nanofacet activators of catalytic materials. That provides a new material design strategy and allows systematic investigation of how catalysis on high-energy surfaces proceeds, with implications for applications in the field.

■ ASSOCIATED CONTENT

Ⓢ **Supporting Information.** Experimental details; XRD, SEM, TEM, and UV—vis spectra of Au NPs. This material is available free of charge via the Internet at http://pubs.acs.org.

■ AUTHOR INFORMATION

Corresponding Authors
flu@bnl.gov; ogang@bnl.gov

■ REFERENCES

(1) (a) Yang, M.; Alvarez-Puebla, R.; Kim, H. S.; Aldeanueva-Potel, P.; Liz-Marzán, L. M.; Kotov, N. A. *Nano Lett.* **2010**, *10*, 4013. (b) Talapin, D. V.; Lee, J. S.; Kovalenko, M. V.; Shevchenko, E. V. *Chem. Rev.* **2010**, *110*, 389. (c) Claridge, A.; Castleman, A. W., Jr.; Khanna, S. N.; Murray, C. B.; Sen, A.; Weiss, P. S. *ACS Nano* **2009**, *2*, 244. (d) Jiang, Z. Y.; Kuang, Q.; Xie, Z. X.; Zheng, L. S. *Adv. Funct. Mater.* **2010**, *20*, 3634.

(2) (a) Tao, A. R.; Sinsermsuksakul, P.; Yang, P. *Nature Nanotechnol.* **2007**, *2*, 435. (b) Niu, W. X.; Zheng, S. L.; Wang, D. W.; Liu, X. Q.; Li, H. J.; Han, S.; Chen, J.; Tang, Z. Y.; Xu, G. B. *J. Am. Chem. Soc.* **2009**, *131*, 697. (c) Millstone, J. E.; Wei, W.; Jones, M. R.; Yoo, H.; Mirkin, C. A. *Nano Lett.* **2008**, *8*, 2526. (d) Personick, M. L.; Langille, M. R.; Zhang, J.; Harris, N.; Schatz, G. C.; Mirkin, C. A. *J. Am. Chem. Soc.* **2011**, *133*, 6170. (e) Niu, W. X.; Xu, G. B. *Nano Today* **2011**, *6*, 265.

(3) Tian, N.; Zhou, Z. Y.; Sun, S. G.; Ding, Y.; Wang, Z. L. *Science* **2007**, *316*, 732.

(4) (a) Ma, Y. Y.; Kuang, Q.; Jiang, Z. Y.; Xie, Z. X.; Huang, R. B.; Zheng, L. S. *Angew. Chem., Int. Ed.* **2008**, *47*, 8901. (b) Zhang, L.; Niu, W. X.; Li, Z. Y.; Xu, G. B. *Chem. Commun.* **2011**, *47*, 10353.

(5) Ming, T.; Feng, W.; Tang, Q.; Wang, F.; Sun, L. D.; Wang, J. F.; Yan, C. H. *J. Am. Chem. Soc.* **2009**, *131*, 16350.

(6) (a) Zhang, J.; Langille, M. R.; Personick, M. L.; Zhang, K.; Li, S. Y.; Mirkin, C. A. *J. Am. Chem. Soc.* **2010**, *132*, 14012. (b) Huang, X. Q.; Zhao, Z. P.; Fan, J. M.; Tan, Y. M.; Zheng, N. F. *J. Am. Chem. Soc.* **2011**, *133*, 4718.

(7) (a) Trong, T.; Lu, X. M. *J. Phys. Chem. C* **2011**, *115*, 3638. (b) Personick, M. L.; Langille, M. R.; Zhang, J.; Mirkin, C. A. *Nano Lett.* **2011**, *11*, 3394.

(8) Zheng, Y.; Tao, J.; Liu, H.; Zeng, J.; Yu, T.; Ma, Y.; Moran, C.; Wu, L.; Zhu, Y.; Liu, J.; Xia, Y. *Small* **2011**, *7*, 2307.

(9) Wang, C.; Daimon, H.; Onodera, T.; Koda, T.; Sun, S. *Angew. Chem., Int. Ed.* **2008**, *47*, 3588.

(10) Fan, F. R.; Liu, D. Y.; Wu, Y. F; Duan, S.; Xie, Z. X.; Jiang, Z. Y.; Tian, Z. Q. *J. Am. Chem. Soc.* **2008**, *130*, 6949.

(11) Lu, C. L.; Prasad, K. S.; Wu, H. L.; Ho, J. A.; Huang, M. H. *J. Am. Chem. Soc.* **2010**, *132*, 14546.

(12) Liu, M. Z.; Guyot-Sionnest, P. *J. Phys. Chem. B* **2005**, *109*, 22192.

(13) Kondo, T.; Morita, J.; Hanaoka, K.; Takakusagi, S.; Tamura, K.; Takahasi, M.; Mizuki, J.; Uosaki, K. *J. Phys. Chem. C* **2007**, *111*, 13197.

(14) Brankovic, S. R.; Wang, J. X.; Adžić, R. R. *Surf. Sci.* **2001**, *474*, L173.

(15) Wang, J. X.; Inada, H.; Wu, L. J.; Zhu, Y. M.; Choi, Y. M.; Liu, P.; Zhou, W. P.; Adzic, R. R. *J. Am. Chem. Soc.* **2009**, *131*, 17298.